

Quantum Mechanical Study of the Structure and Spectroscopic (FTIR, FT-Raman, NMR and UV), First Order Hyperpolarizability and HOMO-LUMO Analysis of 2-[(Methylamino)methyl]Pyridine

S.Seshadri¹, Rasheed .M.P², R.Sangeetha³

¹(Associate Professor and HOD, PG and Research Department of Physics, Urumudhanalakshmi College, Trichy-19)

^{2,3}(Research Scholar, PG and Research Department of Physics, Urumudhanalakshmi College, Trichy-19)

Abstract: In this study, geometrical optimization, spectroscopic analysis, electronic structure and nuclear magnetic resonance studies of 2-[(methylamino)methyl]pyridine (abbreviated as 2MAMP) were investigated by utilizing DFT/B3LYP with 6-31G (d,p) as basis set. The FTIR and FT-Raman spectra of 2-[(methylamino)methyl]pyridine (2MAMP) have been recorded in the region 4000–400 cm⁻¹ and 4000–50 cm⁻¹ respectively. Complete vibrational assignments, analysis and correlation of the fundamental modes for the title compound were carried out. The harmonic vibrational frequencies were calculated and scaled values have been compared with experimental FTIR and FT-Raman spectra. The observed and calculated frequencies are found to be in good agreement. The theoretical UV-Visible spectrum of the compound was performed by Time Dependent DFT (TD-DFT) approach. The ¹H and ¹³C nuclear magnetic resonance (NMR) chemical shifts of 2MAMP were calculated using the GIAO method by applying B3LYP method. The dipole moment, polarizability and first order hyperpolarizability and Mulliken charges of the molecule were calculated using DFT calculations. The polarizability and first hyperpolarizability of the studied molecule indicate that the compound is a good candidate of nonlinear optical materials. The Chemical reactivity and Thermodynamic properties of 2MAMP at different temperatures were also calculated. In addition, molecular electrostatic potential (MEP), frontier molecular orbitals (FMO) analysis were investigated using theoretical calculations. The calculated HOMO and LUMO energies show that charge transfer occurs within the molecule.

Keywords: FTIR; FT-RAMAN; UV-Vis; NMR; Hyperpolarizability; 2MAMP

I. Introduction

The nonlinear optical responses induced in various materials are of great interest in recent years because of the applications in photonic technologies such as optical communications, data storage and image processing. In recent years, the synthetic approaches to various pyridine derivatives and their biological activity were studied. Analysis of the scientific and patent literature indicates that the amino group is used to create a wide range of the drugs and products for agriculture [1,2]. Some pyridine derivatives are patented and widely used in medicine as the anti androgenic and hypotensive drugs [3]. Antimicrobial preparations based on pyridine derivatives are of great interest and are used in medicine and in agriculture [4]. 2-[(methylamino)methyl]pyridine is a pyridine derivative. Our molecule 2MAMP has the following properties: Pale yellow color, liquid form; Boiling point: 178.91 °C [5]

II. Experimental details

The fine sample of 2MAMP was obtained from Sigma Aldrich, UK, and used as such for the spectral measurements. The room temperature FTIR spectrum of the compound was measured in the 4000–400 cm⁻¹ region at a resolution of ±1 cm⁻¹, using a BRUKER IFS-66V vacuum Fourier transform spectrometer equipped with a Mercury Cadmium Telluride (MCT) detector, a KBr beam splitter and global source.

The FT-Raman spectrum of 2MAMP was recorded on a BRUKER IFS-66V model interferometer equipped with an FRA-106 FT-Raman accessory. The spectrum was recorded in the 4000–50 cm⁻¹ Stokes region using the 1064 nm line of a Nd:YAG laser for the excitation operating at 200 mW power. The reported wavenumber are expected to be accurate to within ±1 cm⁻¹.

III. Computational details

The quantum chemical calculation of 2MAMP has been performed with the standard Density Functional Triply-Parameter Hybrid model DFT/B3LYP. The 6-31G(d,p) basis set have been employed (the valence triple basis set, augmented by d-polarization functions on carbon and nitrogen, p-polarization functions on hydrogen atoms and enlarged by diffuse functions on all atoms) using the Gaussian 09 program [6]. The

optimized geometry corresponding to the minimum on the potential energy surface have been obtained by solving self consistent field equation iteratively. Harmonic vibrational wavenumbers have been calculated using analytic second derivatives to confirm the convergence to minima on the potential energy surface and to evaluate the zero-point vibrational energy [7]. Multiple scaling of the force field has been performed by the SQM procedure [8,9] to offset the systematic errors caused by basis set incompleteness, neglect of electron correlation and vibrational anharmonicity [10]. These force fields obtained in Cartesian coordinates and dipole derivatives with respect to atomic displacements were extracted from the archive section of the Gaussian 09 output and transformed to a suitably defined set of internal coordinates (the 'natural coordinates'). Normal coordinate analysis on 2MAMP has been performed to obtain full description of the molecular motion pertaining to the normal modes using the MOLVIB-7.0 program [11,12].

IV. Prediction of Raman intensities

The Raman activities (S_i) calculated with the GAUSSIAN 09 program and adjusted during the scaling procedure with MOLVIB were subsequently converted to relative Raman intensities (I_i) using the following relationship derived from the basic theory of Raman scattering [13,14].

$$I_i = \frac{f(v_o - v_i)^4 S_i}{v_i \left[1 - \exp\left(\frac{-hcv_i}{kT}\right) \right]}$$

where v_o is the exciting frequency (in cm^{-1} units); v_i is the vibrational wave number of the i^{th} normal mode, h , c and k are fundamental constants and f is a suitably chosen common normalization factor for all peaks intensities. Raman activities and calculated Raman intensities are reported in TABLE 5

V. Results and discussion

5.1 Thermodynamic analysis

The molecule taken for this investigation has a great deal of interest in thermodynamic property analysis. Based on the vibrational analysis of title molecule at B3LYP/6-31 G(d,p) basis set, the thermodynamic parameters such as heat capacity at constant volume (C_v), Entropy (S), enthalpy change (ΔH) were calculated for different temperatures and listed in the TABLE 1.

it can be seen that, when the temperature increases from 100 to 1000 K the thermodynamic functions like Specific heat capacity at constant volume (C_v), Entropy (S) and enthalpy (ΔH) are also increases, because molecular vibrational intensities increase with temperature [15]. The entropy and enthalpy changes revealed that the molecule possesses more flexibility of changing its own thermodynamic system with respect to the temperature. Fitting factor of the thermodynamic functions such as heat capacity, entropy and enthalpy changes are 0.978, 0.967 and 0.976 respectively. The correlation graphics of temperature dependence of thermodynamic functions for 2MAMP molecule are shown in Figures 1.

TABLE 1-The Temperature dependence of Thermodynamic parameters of 2MAMP

Temperature [T]	Energy [E] (KCal/Mol)	Heat capacity [Cv] (Cal/Mol-Kelvin)	Entropy [S] (Cal/Mol-Kelvin)	Enthalpy change
100	92.056	14.372	67.422	0.147018
200	102.422	21.131	78.998	0.163853
300	107.278	31.036	90.854	0.171908
400	110.898	41.287	101.768	0.177993
500	115.499	50.496	112.441	0.185642
600	120.946	58.213	122.714	0.194641
700	127.097	64.597	132.489	0.204759
800	133.83	69.916	141.737	0.215806
900	141.052	74.396	150.472	0.227631
1000	148.687	78.203	158.722	0.240115

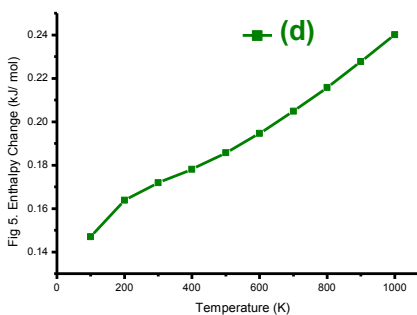
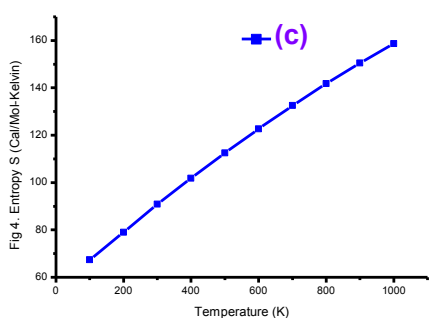
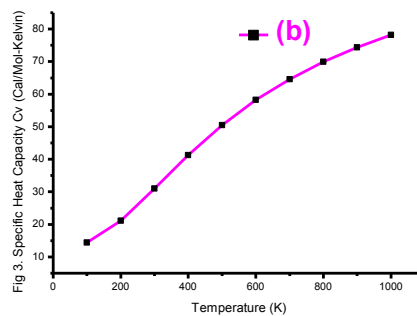
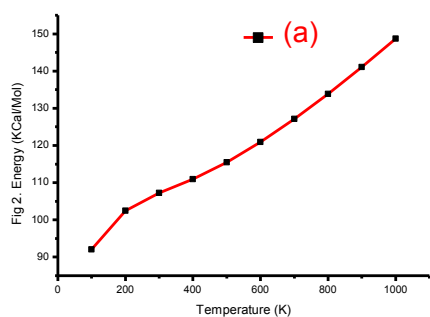


Fig 1. (a). Temperature dependence of Energy 2MAMP
 (b). Temperature dependence of Heat Capacity At Constant Volume of 2MAMP
 (c). Temperature dependence of Entropy of 2MAMP
 (d). Temperature dependence of Enthalpy Change of 2MAMP

The zero point vibrational energy and rotational constants in GHz obtained for optimized geometry with B3LYP/6-31 g(d,p) basis set are presented in TABLE2. While performing DFT Calculations the molecule was considered to be at room temperature (298.15K) and at a pressure of 1atm.

TABLE 2-The calculated Thermodynamical parameters of 2MAMP

Parameters	B3LYP/6-31G(d,p)
Zero-point vibrational energy (Joules/Mol)	370558.4
Rotational constants (GHz):	A 1.8595103
	B 1.1246245
	C 0.7123078

5.2 Molecular geometry

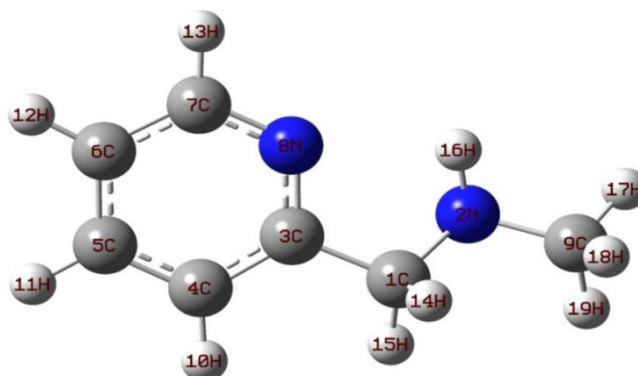


Fig 2. Optimized Structure of 2MAMP along with numbering of atoms

The labeling of atoms of the title compound is shown in Figure 2. The global minimum energies obtained by the DFT structure optimization for 2MAMP for B3LYP/6-31G(d,p) , B3LYP/6-311+G(d,p), and

B3LYP/6-311G++(d,p) basis sets respectively are presented in TABLE 3. This energy difference is clearly understandable, since the molecules are under different environments.

TABLE 3-Total energies (in Hartrees) based on B3LYP/6-31 g(d,p) , B3LYP/6-311 + G(d,p) and B3LYP/6-311 + +G(d,p) basis sets for 2MAMP

Basis set	2-[(methylamino)methyl]pyridine
B3LYP/6-31 G(d,p)	-382.27072686
B3LYP/6-311+ G(d,p)	-382.32631108
B3LYP/6-311++ G(d,p)	-382.32646453

The optimized geometrical parameters like bond length, bond angles and dihedral angles are presented in TABLE 4.

TABLE 4-Optimized geometrical parameters of 2MAMP obtained by B3LYP/6-31 g(d,p) density functional calculations

Bond length	Value(Å)	Bond angle	Value(°)	Torsional angle	Value(°)
N2-H16	1.017362	C4-C5-C6	118.83	H16-N2-C1-C3	-44.25
C4-H10	1.085747	H16-N2-C9	110.71	H10-C4-C3-C1	2.46
C5-H11	1.086268	H10-C4-C5	120.91	H11-C5-C6-C7	-180.41
C6-H12	1.085155	H11-C5-C6	120.7	H12-C6-C7-N8	-179.83
C1-H15	1.097911	H12-C6-C7	120.47	H15-C1-C3-C4	-18.33
C7-H13	1.088678	H15-C1-H14	106.02	H13-C7-N8-C3	-180.39
C9-H17	1.094049	H13-C7-N8	116.03	H17-C9-N2-C1	-184.36
C9-H19	1.096814	H17-C9-H19	107.44	H19-C9-N2-C1	-66.57
C1-H14	1.111082	H19-C9-H18	107.22	H14-C1-C3-C4	-263.41
C9-H18	1.106854	H14-C1-N2	112.53	H18-C9-N2-C1	54.03
N8-C7	1.337509	H18-C9-H17	108.17	N8-C7-C6-C5	0.42
C4-C5	1.392815	N8-C7-C6	123.61	C4-C5-C6-C7	0.03
C6-C5	1.394179	C7-C6-C5	118.03	C3-N8-C7-C6	-0.51
C7-C6	1.394431	C3-N8-C7	118.26	N2-C1-C3-C4	-139.7
N8-C3	1.342382	N2-C1-C3	111.21	C9-N2-C1-C3	-166.6
N2-C1	1.455141	C9-N2-C1	113.1	C1-C4-N8-C3	1.6
N2-C9	1.454524	C1-C3-N8	115.96		
C1-C3	1.515334				

For numbering of atoms refer Fig. 1

2MAMP belongs to C_1 point group symmetry with 19 atoms composing the structure. The molecule has 51 fundamental modes of vibration. From the structural point of view of the molecule 2MAMP has 35 in plane and 16 out of plane vibrations.

Total number of fundamental modes of vibration, $51 (\Gamma_{\text{vib}}) = 35 A'(\text{in-plane}) + 16 A''(\text{out-of-plane})$

5.3 Assignment of spectra

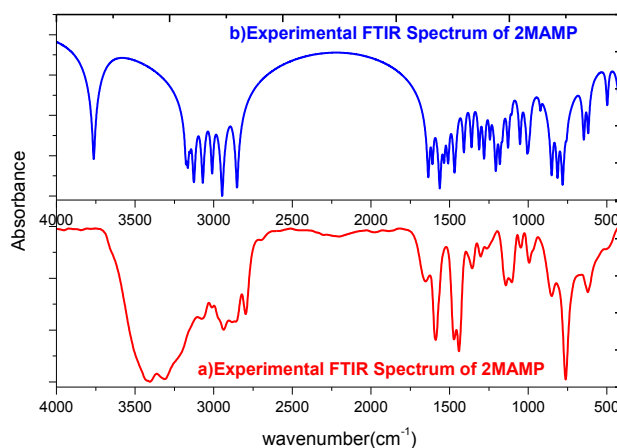


Fig 3. Comparison of Theoretical and experimental FT-IR spectrum of 2MAMP

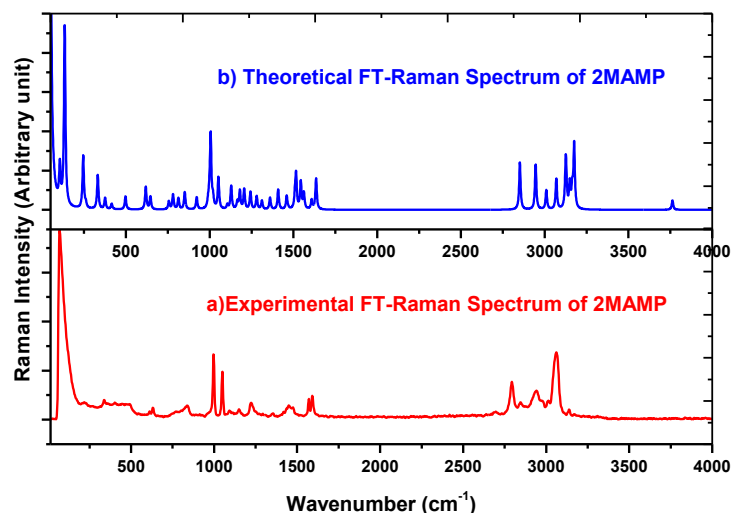


Fig 4. Comparison of Experimental and Theoretical FT-Raman spectrum of 2MAMP

Detailed description of vibrational modes can be given by means of normal coordinate analysis. The observed and calculated frequencies, calculated IR, Raman and normal mode descriptions (characterized by PED) are reported in TABLE 5 for 2MAMP. The observed and simulated FT-IR and FT-Raman spectra of 2MAMP are presented in Figure 3 and Figure 4 respectively. When using computational methods to predict theoretical normal vibrations for relatively complex poly atomic structures scaling strategies are used to bring computed wave numbers into closer agreement with observed frequencies using the latest version of MOLVIB program .

TABLE 5- Assignment of fundamental vibrations of 2MAMP by normal mode analysis based on SQM force field calculations using selective scaled B3LYP/6-31g(d,p)

No	symmetry species	Observed frequency		Calculated using B3LYP/6-31 G(d,p) force field Freq					Characterisation of normal modes with PED%
		IR (cm ⁻¹)	Raman (cm ⁻¹)	Unscaled (cm ⁻¹)	Scaled (cm ⁻¹)	IR intensity (K mol ⁻¹)	Raman activity Si	Raman intensity (Ii)	
1	A	3780.0	-	3523.4	3763	13.84	58.50	75.41	vNH (100)
2	A	-	-	3212.3	3176	15.52	232.33	408.42	vCH (99)
3	A	-	-	3200.5	3164	19.86	65.65	116.81	vCH (99)
4	A	-	-	3185.5	3150	4.66	86.34	155.98	vCH (99)
5	A	-	-	3163.2	3128	24.30	101.17	187.00	vCH (99)
6	A	-	3138.1	3111.9	3124	33.35	98.99	192.90	vCHMEL (99)
7	A	-	3061.2	3056.8	3069	56.91	105.00	216.67	vCHMEL (99)
8	A	-	3013.5	3043.7	3010	29.99	53.32	111.55	vCH (99)
9	A	-	2941.7	2934.2	2946	119.03	135.35	317.84	vCHMEL (99)
10	A	-	2845.4	2884.1	2852	70.51	119.91	297.09	vCH (99)
11	A	1652.0	-	1650.1	1635	46.43	19.65	231.43	vCC (41), vCN (30), bCH (14)
12	A	-	1591.4	1629.7	1599	16.38	10.00	121.56	vCC (48), vCN (22), bCH (13)
13	A	-	1570.3	1532.3	1562	13.30	26.26	373.12	bCNH (67)
14	A	-	-	1523.4	1544	10.50	5.80	83.65	gCH3 (86)
15	A	-	-	1516.4	1535	30.97	4.56	66.57	bCH (41), vCC (24), vCN(19)
16	A	-	-	1506.6	1516	10.39	12.79	189.64	gCH3 (92),
17	A''	-	-	1497.8	1509	26.43	16.26	244.64	bCH (52), tbutte (24)
18	A	1471.0	-	1475.5	1468	43.98	1.40	21.86	bCH(42), vCC (20), gCH3 (11)
19	A	-	1449.6	1469.6	1453	3.06	10.42	164.36	gCH3 (43), bCH3 (35), bCH (11)
20	A	-	-	1392.3	1409	5.34	7.97	143.67	bCCH (34), gCN (14)
21	A	1356.0	-	1332.7	1360	8.80	6.00	120.42	bCH (34), vCN (29), bNCH (11)
22	A	1302.0	-	1308.5	1312	0.74	2.88	60.34	vCC (45), vCN (34), bCH (12)
23	A	1263.0	-	1269.6	1281	15.46	8.08	182.27	gCN (26), bCCH(24), gCH3 (10)
24	A	-	1222.7	1249.3	1243	8.73	11.49	269.43	vCN (35), vCC (24)
25	A	-	-	1195.4	1206	6.08	4.35	113.30	vCN (48), vCC (19)

26	A	-	-	1180.0	1180	6.64	4.02	108.17	vCN (29), gCH3(16), bCH3(15)
27	A	-	-	1162.6	1165	37.69	6.96	193.77	bCH (57), vCC (31)
28	A	-	1149.7	1150.1	1128	2.84	10.47	299.25	bCH3 (56), gCH3 (22)
29	A	1104.0	-	1120.7	1105	0.31	2.01	61.19	vCC (38), bCH (37)
30	A	-	1049.6	1075.7	1052	4.48	15.78	527.69	vCC (65), bCH (15), bring (14)
31	A"	-	-	1017.0	1029	1.58	9.03	344.41	gCH (88), tring (12)
32	A	-	-	1007.8	1020	1.07	2.36	91.82	gCN (38), bCCH (13), gCH (13)
33	A	-	-	1005.2	1006	4.03	7.74	303.20	bring (45), vCN (17), CC (16)
34	A	-	996.8	997.8	999	7.19	6.23	248.46	bCH3(24), vCN (23), gCH3 (10)
35	A"	993.0	-	973.3	991	0.30	1.18	49.87	gCH (65), gCN (16), tring (10)
36	A	-	-	906.1	923	0.60	3.64	181.22	gCH (90)
37	A"	850.0	-	859.1	851	32.37	5.06	284.13	vCC (22), vCN (13) tbutte (16)
38	A"	-	837.7	812.1	833	51.63	4.15	264.55	gNH(20), gCN (16),tbutte (11)
39	A	-	-	770.9	781	55.21	2.96	211.89	gCH (72)
40	A"	761.0	-	758.3	756	1.55	1.63	120.97	tring (67), gCC (14), gCH (10)
41	A"	-	-	649.4	646	4.81	2.65	277.58	bring (55), tring (8)
42	A"	621.0	-	622.7	618	3.44	3.44	396.02	bring (67), tring (5), CC (5)
43	A"	-	-	496.6	497	0.56	1.68	314.92	tring (43), gCC (29), gCH (11)
44	A"	411.0	-	416.6	415	2.32	0.52	141.95	tring (85), gCH (14)
45	A"	-	-	377.1	376	2.26	0.74	248.64	bCC (11), bNCC(11) tring (18)
46	A	-	337.7	337.3	332	0.89	2.47	1055.90	bCNC(40), CC (15)
47	A"	-	-	253.9	261	1.62	0.23	176.87	tCH3 (84)
48	A"	-	217.8	244.9	245	0.27	2.20	1834.45	tring(37), bCNC(14), gCN(10)
49	A"	-	-	133.7	135	0.76	2.66	7678.19	gCN (16),tring (16), bCCH (15)
50	A"	-	-	105.1	105	4.36	0.36	1708.95	tCN(34), gCN0 (18), tCC(10)
51	A"	-	69.5	43.8	53	2.06	2.51	69290.8	tCC (50), tCN (20), gCN (10)

(v) stretching; (b) bending; (g) scissoring and wagging ; (t) torsion ;(tbutte) Butterfly PED values greater than 10% are given

The RMS error between unscaled (B3LYP/6-31 G(d,p)) and experimental frequencies is found to be 39.7 cm⁻¹. Root mean square value is obtained in the study using the following expression

$$RMS = \sqrt{\frac{1}{n-1} \sum_i^n (v_i^{calcu} - v_i^{exp})^2}$$

This is quite obvious since the frequencies calculated on the basis of quantum mechanical force fields usually differ appreciably from observed frequencies. This is partly due to the neglect of anharmonicity and partly due to the approximate nature of the quantum mechanical methods. In order to reproduce the observed frequencies, refinement of scaling factors are applied and optimized via least square refinement algorithm which resulted in a weighted RMS deviation of 10.15 cm⁻¹ between the experimental and scaled frequencies.

For 2MAMP, a multiple scale factors are applied in the normal coordinate analysis and the subsequent least square fit refinement, results into the very close agreement between the observed fundamentals and the scaled frequencies (Table 5). Refinement of the scaling factor applied in this study achieved a weighted mean deviation of 4.27 cm⁻¹ between the experimental and SQM frequencies [16-18]. It is convenient to discuss the vibrational spectra of 2MAMP in terms of characteristic spectral regions as described below.

5.3.1 C-H vibration

Most organic molecules contain alkane residues and their general appearance may be seen in the infrared spectrum. The strong absorption band generally centered around 2925 cm⁻¹ represents the C-H stretching absorption of methylene [19] group. Most of the time, it is sufficient to locate the mean position of this aliphatic C-H stretch. In fact, the C-H stretching modes of methylene have asymmetric and symmetric C-H stretching modes and these give four absorption bands just below 3100 cm⁻¹. In our title compound, calculated bands appeared at 3212, 3200.5, 3185, 3163, 3044 and 2884 cm⁻¹ in DFT method have been assigned to C-H asymmetric and symmetric stretching vibrations. The FT-Raman bands at 3013 and 2845 represent C-H stretching vibration. The calculated wavenumber for these modes are scaled to 3010 and 2852 cm⁻¹ respectively. The in-plane and out-of-plane bending vibrations of methyl group have also been identified for the title compound and they are presented in [Table 5](#).

5.3.2. C-N vibrations

The C-N stretching frequency is a rather difficult task since the mixing of several bands is possible in this region. In our present work, the band observed at 1652 in FTIR spectrum and 1591 in Raman spectrum have been attributed to C-N vibrations. The theoretically computed value of the corresponding C-N stretching vibrations is predicted at 1650 and 1629 cm^{-1} respectively. These vibrations are mixed with C-C stretching and C-H bending vibration as evident from the last column of PED. In this work, the peaks identified at 1356 and 1302 cm^{-1} in IR have been assigned to C-N stretching absorption bands.

5.3.3 N-H vibrations

Heterocyclic compounds containing an N-H group exhibit N-H stretching absorption in the region from 3500 to 3200 cm^{-1} [20] and a weak band at 3100–3070 cm^{-1} for an overtone of the N-H band [21]. The position of absorption depends upon the degree of hydrogen bonding and hence upon the physical state of the sample [22]. For the title compound, the very strong band observed at 3780 cm^{-1} in the IR spectrum is assigned as N-H stretching mode. The calculated wavenumber for this mode is at 3523 cm^{-1} in B3LYP method. This mode is a pure stretching mode, and as it is evident from the PED column they are almost contributing 100%. The wavenumber (3523 cm^{-1}) computed by B3LYP/6-31G(d,p) method shows the deviation (257 cm^{-1}) when compared with experimental IR data (3780 cm^{-1}). This may be due to intermolecular hydrogen bonds in solid state between the NH group and the N atom present in the ring. This is the reason for the downshift of NH band at 3523 cm^{-1} . The N-H in-plane bending mode observed at 1570 cm^{-1} in FT-Raman spectrum. The calculated wavenumber for this mode is at 1629.7 cm^{-1} at B3LYP method and it is scaled to 1599 cm^{-1} . Theoretically predicted values are coinciding very well with the observed frequencies. The TED corresponding to this vibration suggests that it (mode.No.13) is a medium mode and exactly contributing to 67% (Table 5).

The weak N-H out of plane bending mode observed at 837 cm^{-1} in FT-Raman spectrum. The calculated wavenumber for this mode is at 812 cm^{-1} at B3LYP method and it is scaled to 833 cm^{-1} . Theoretically predicted values are coinciding very well with the observed frequencies. The TED corresponding to this vibration suggests that it (mode.No.38) is a weak mode and exactly contributing to 20% (Table 5).

5.3.4. CH₃ Vibration

The CH₃ stretching and bending modes appear to be quite pure group vibrations. Two asymmetric and one symmetric stretching vibrations of CH₃ group are usually observed in the range 2990–3050 cm^{-1} [23,24]. In the present case of our molecule, there is only a single CH₃ group. The asymmetric stretching vibrations of CH₃ groups observed at 3138 and 3061 cm^{-1} in FT-Raman spectrum. The calculated wavenumber for these modes are at 3111.9 and 3057 cm^{-1} at B3LYP method and they are scaled to 3124 and 3069 cm^{-1} respectively. Theoretically predicted values are coinciding very well with the observed frequencies. The TED corresponding to these vibrations suggest that they are (mode.No.6 and 7) very strong modes and exactly contributing to 99% (Table 5).

The symmetric stretching vibrations of CH₃ group have been identified at 2934.2 cm^{-1} in DFT method. Symmetric stretching band observed in the FT-Raman spectrum of methyl group at 2941.7 cm^{-1} and it is scaled to 2946 cm^{-1} . The in-plane bending vibration of the CH₃ group is identified at 1523, 1506.6, 1475 and 1469.6 cm^{-1} in DFT method. The assignment of the band at 253.9 cm^{-1} in DFT method is attributed to the torsion CH₃ (tCH₃). The bands at 1471 cm^{-1} in FT-IR spectrum and 1449.6 cm^{-1} in FT-Raman spectrum represent in-plane and out of plane bending vibrations of CH₃ and these bands are scaled to 1468 and 1453 cm^{-1} respectively.

5.4 Frontier molecular orbitals

Many organic molecules that contain conjugated π -electrons are characterized as hyperpolarizabilities and are analyzed by means of vibrational spectroscopy [25,26]. Both the Highest Occupied Molecular Orbital (HOMO) and the Lowest Unoccupied Molecular Orbital (LUMO) are the main orbital taking part in chemical reaction. The HOMO energy characterizes the ability of electron giving, the LUMO characterizes the ability of electron accepting, and the gap between HOMO and LUMO characterizes the molecular chemical stability [27]. The energy gap between the HOMOs and LUMOs called as energy gap is a critical parameter in determining molecular electrical transport properties because it is a measure of electron conductivity [28]. Surfaces for the frontier orbital's were drawn to understand the bonding scheme of present compound. The features of these MO can be seen in Figure 5.

This electronic absorption corresponds to the transition from the ground state to the first excited state and is mainly described by one electron excitation from HOMO to LUMO. While the energy of the HOMO is directly related to the ionization potential, LUMO energy is directly related to the electron affinity.

There are lots of applications available for the use of HOMO and LUMO energy gap as a quantum chemical descriptor. It establishes correlation in various chemical and bio-chemical systems [29]. The HOMO–

LUMO energy gap is an important value for stability index. A large HOMO–LUMO gap implies high stability for the molecule in the sense of its lower reactivity in chemical reactions [30]. According to B3LYP/6-31G(d,p) calculation, the energy band gap (translation from HOMO to LUMO) of the molecule is about -5.02608 eV

HOMO energy = - 5.69710 eV
 LUMO energy = - 0.67102 eV
 HOMO – LUMO energy gap = - 5.02608 eV

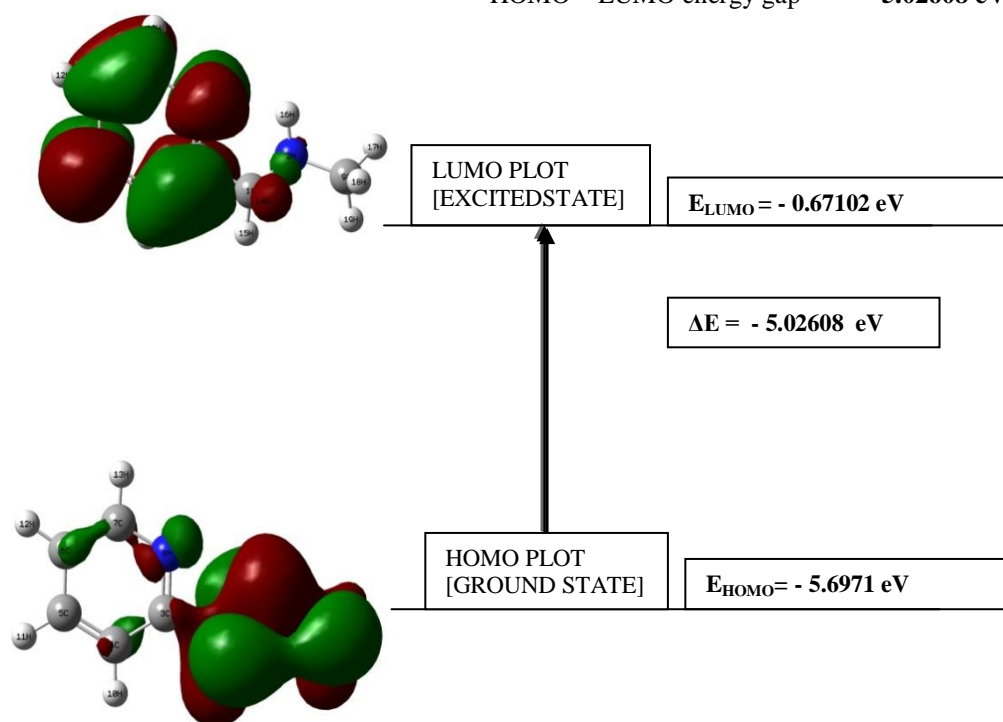


Fig 5. Homo LUMO plot of of 2MAMP

5.5. ¹³C and ¹H NMR spectral analysis

Recently, Gauge Invariant Atomic Orbital's (GIAO) NMR DFT calculations have become popular [31] and can successfully predict the chemical shift (δ, ppm) for small isolated molecules [32-34]. However, the accuracy of NMR theoretical predictions depend on the implemented basis set, and optimized structural parameters. Earlier investigations favor DFT predictions over the RHF method [35]. Therefore, structural parameters obtained with the hybrid B3LYP functional at the 6-31G(d,p) level of theory were used to predict ¹H and ¹³C chemical shifts utilizing the recommended GIAO approach [36]. The theoretically computed ¹³C and ¹H NMR spectrum are shown in Figure 6. Chemical shifts were reported in parts per million relative to TMS. Relative chemical shifts were estimated by using the corresponding TMS shielding calculated in advance at the same theoretical level as the reference. Aromatic carbons give signals in overlapped areas of the spectrum with chemical shift values from 100 to 150 ppm [37,38]. It can be seen from Table 6, that due to the influence of electronegative nitrogen atom, the chemical shift value of carbon atoms are significantly differing the shift positions in the range 150–180 ppm. Thus, the C2 atom has its chemical shifts at 154.728 ppm. The chemical shift values of H atoms in methyl group are quite low (≤3ppm) due to the shielding effect. The chemical shift values of Carbon and Hydrogen atoms are reported in TABLE 6.

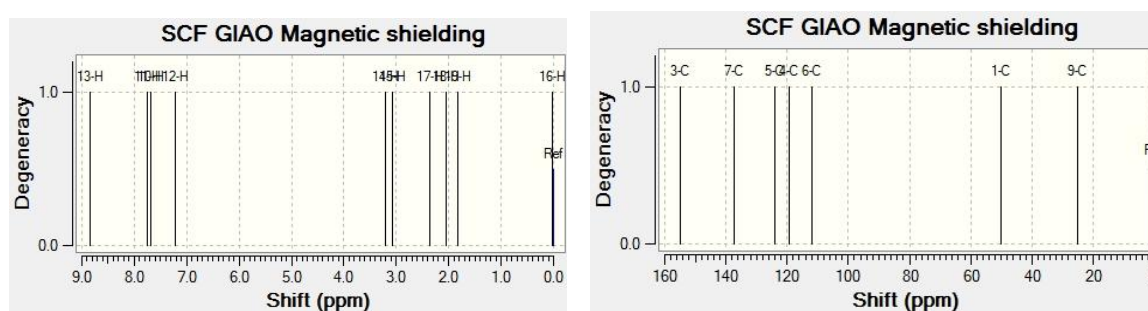


Fig 6. Theoretically calculated NMR Spectrum of ¹H and ¹³C of 2MAMP

TABLE 6. Theoretical isotropic chemical shift calculated using DFT B3LYP/6-31 G(d,p) (with respect to TMS, All values in ppm) for 2MAMP

Calculated chemical shift (ppm)	
Atom	B3LYP/6-31G(d,p)
C1	50.2443
C3	154.728
C4	119.2912
C5	123.9322
C6	111.9734
C7	137.3252
C9	25.2256
H10	7.676
H11	7.7616
H12	7.2183
H13	8.8536
H14	3.1978
H15	3.0828
H16	0.0178
H17	2.3659
H18	2.0451
H19	1.8323

5.6 Mulliken charges

Mulliken atomic charge calculation [39] has an important role in the application of quantum chemical calculation to molecular system. The atomic charge in molecules is fundamental to chemistry. For instance, atomic charge has been used to describe the processes of electronegativity equalization and charge transfer in chemical reactions [40,41], and to model the electrostatic potential outside molecular surfaces [42-44]. Mulliken atomic charges calculated at the B3LYP/6-31 G(d,p) level by determining the electron population of each atom as defined by the basis function is collected in **TABLE 7** along with the natural atomic charges obtained in NBO analysis. The carbon atoms C4 (0.4255) has the highest positive charge when compared with all other carbon atoms as shown in the histogram. Moreover, hydrogen atom connected to Nitrogen atom has the maximum positive charges H16 (0.2875), at the DFT calculation this is due to the reason of electro negative nitrogen of the NH group. The NH group of Nitrogen atom N2 (-0.2843) has the bigger negative charges compare to other the Nitrogen atom inside the pyridine ring of given molecule. Illustration of atomic charges plotted at 6-31G(d,p) level has been shown in **Figure.7** and the histogram of calculated mulliken charges and natural atomic charges of 2MAMP is shown in **Figure .8**

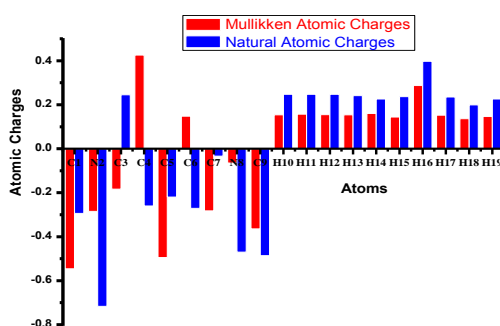
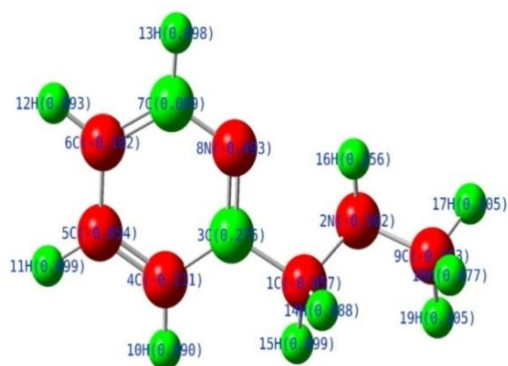


Fig 7. Illustration of mullikken atomic charges **Fig 8.** The histogram of calculated Mulliken charges And Natural atomic charges of 2MAMP

TABLE 7. Atomic charges for optimized geometry of 2MAMP using DFT B3LYP/6-31g(d,p)

Atomic Number	2-[(methylamino)methyl]pyridine	
	Mulliken atomic charges	Natural atomic charges
C1	-0.54541	-0.29418
N2	-0.28433	-0.71621
C3	-0.18392	0.24539
C4	0.425594	-0.26011
C5	-0.4946	-0.21953
C6	0.147847	-0.27091
C7	-0.28241	-0.03334
N8	-0.06508	-0.47017
C9	-0.36418	-0.48562
H10	0.154311	0.24724
H11	0.156822	0.24787
H12	0.154531	0.24754
H13	0.15393	0.24112
H14	0.160104	0.22578
H15	0.144008	0.23696
H16	0.287578	0.39737
H17	0.152466	0.23531
H18	0.136146	0.19957
H19	0.14658	0.22591

5.7 UV-Vis spectral analysis

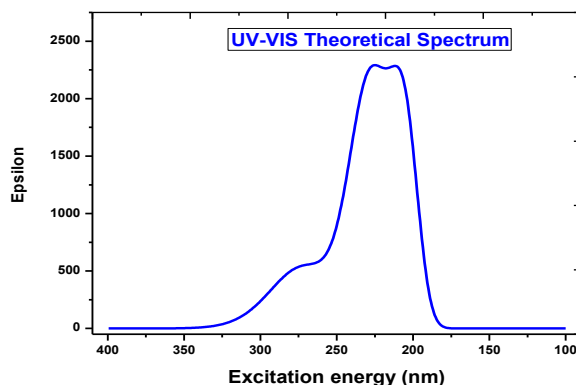


Fig.9. The UV-Visible spectrum of 2MAMP

The Time Dependent Density Functional Density (TD-DFT) Calculation has been performed for 2MAMP on the basis of fully optimized ground state structure to investigate the electronic absorption properties. TD-DFT is able to detect accurate absorption wavelengths at a relatively small computing time which correspond to vertical electronic transitions computed on the ground state geometry, especially in the study of solvent effect [45–47]; Thus TD-DFT method is used with B3LYP function and 6-31G(d,p) basis set for vertical excitation energy of electronic spectra. The calculated visible absorption maxima of wave length λ which are a function of the electron availability have been reported in Table 8. The excitation energies, wave length and oscillator strengths for the title molecule at the optimized geometry in the ground state were obtained in the frame work of TD-DFT calculations with the B3LYP/6-31G(d,p) method. TD-DFT methods are computationally more expensive than semi-empirical methods but allow easily studies of medium size molecules [48,49]. The computed UV spectra predicts one intense electronic transition at 230.9 nm with an oscillator strength $f = 0.0453$ a.u and another electronic transition at 206.23 nm with an oscillator strength $f = 0.0417$ a.u .Calculations of molecular orbital geometry show that the visible absorption maxima of title molecule correspond to the electron transition between frontier orbitals such as transition from HOMO to LUMO. The λ_{\max} is a function of substitution. The stronger the donor character of the substitution, the more electrons pushed into the molecule, the larger λ_{\max} . These values may be slightly shifted by solvent effects. The role of substituent and role of the solvent influence the UV-Visible spectrum. This band may be due to

electronic transition of the ring to methyl group (transition of π - π^*). Both the (HOMO) and (LUMO) are the main orbitals that take part in chemical stability [50].

The theoretical electronic excitation energies, wavelength of the excitation and oscillator strengths were calculated and listed in **TABLE 8** and the Theoretical UV-Visible spectrum is shown in **Figure.9**

TABLE 8. Theoretical electronic absorption spectra values of 2MAMP

Excited State	Energy (eV)	Wavelength λ (nm)	Oscillator strengths (f)
Excited State:1	4.4126	280.98	0.0080
Excited State:2	4.6689	265.55	0.0022
Excited State:3	4.6772	265.08	0.0036
Excited State:4	4.9123	252.39	0.0010
Excited State:5	5.3695	230.94	0.0453
Excited State:6	5.5589	223.04	0.0045
Excited State:7	5.8793	210.88	0.0077
Excited State:8	6.0124	206.23	0.0417

5.8 Analysis of molecular electrostatic surface potential

The molecular electrostatic surface potential provides a visual method to understand the relative polarity of compounds [51]. The electrostatic potential generated in space by charge distribution is helpful to understand the electrophilic and nucleophilic regions in the title molecule. Electrostatic potential map illustrates the charge distributions of the molecule three dimensionally. Knowledge of the charge distributions can be used to determine how molecules interact with one another. One of the purposes of finding the electrostatic potential is to find the reactive site of a molecule [52,53]. In the electrostatic potential map, the semispherical blue shapes that emerge from the edges of the above electrostatic potential map are hydrogen atoms. The molecular electrostatic potential (MEP) at a point r in the space around a molecule (in atomic units) can be expressed as

$$V(r) = \sum_A \frac{Z_A}{|\vec{R}_A - \vec{r}|} - \int \frac{\rho(\vec{r}')}{|\vec{r}' - \vec{r}|} d\vec{r}'$$

Where Z_A is the charge of nucleus A located at R_A , $\rho(\vec{r}')$ is the electronic density function of the molecule, and \vec{r}' is the dummy integration variable

The first and second term represent the contributions to the potential due to nuclei and electron respectively. $V(r)$ is the net resultant electrostatic effect produced at the point r by both the electrons and nuclei of the molecule.

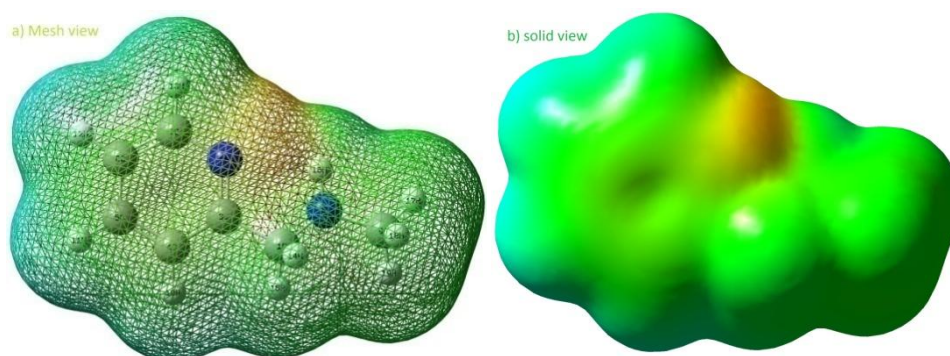


Fig 10. Total electron density isosurface mapped with molecular electrostatic potential of 2MAMP

These two figures, **Figure.10 (a)** mesh view and **(b)** solid view illustrate an electrostatic potential model of the compound computed at the 0.002a.u isodensity surface. The electrostatic potential contour map of positive and negative potential is shown in **Figure 11**.

Molecular electrostatic surface potential (MESP) at a point in a space around a molecule gives an indication of the net electrostatic effect produced at that point by total charge distribution (electron +nuclei) of the molecule and correlates with dipole moments, electro negativity, partial charges and chemical reactivity of the molecule. Potential increases in the following order with respect to the colour. Red < yellow < green < blue. That is negative region (blue and yellow) are related to electrophilic reactivity The maximum positive regions are localized on the Nitrogen atom of ring which can be considered as possible sites for nucleophilic attack. That is negative potential sites are on the electronegative atoms while the positive potential sites around the hydrogen and carbon atoms. Green area covers parts of the molecule where electrostatic potentials are nearly

equal to zero (C-C bond). This is a region of zero potential enveloping the π systems of aromatic ring leaving a more electrophilic region in the plane of hydrogen atom.

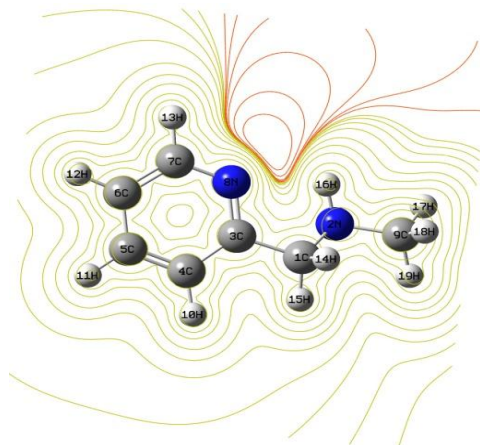


Fig 11. Contour map of molecular electrostatic potential surface

VI. Global reactivity descriptors

By using HOMO and LUMO energy values for a molecule, the global chemical reactivity descriptors of molecules such as hardness (η), chemical potential (μ), softness (S), electronegativity (χ) and electrophilicity index (ω) have been defined [54,55]. On the basis of E_{HOMO} and E_{LUMO} , these are calculated using the below equations.

Using Koopman's theorem for closed-shell molecules, The hardness of the molecule is [56]

$$\eta = (I - A) / 2$$

The chemical potential of the molecule is

$$\mu = -(I + A) / 2$$

The softness of the molecule is

$$S = 1/2\eta$$

The electronegativity of the molecule is

$$\chi = (I + A) / 2$$

The electrophilicity index of the molecule is

$$\omega = \mu^2 / 2\eta$$

Where A is the ionization potential and I is the electron affinity of the molecule. I and A can be expressed through HOMO and LUMO orbital energies as $I = -E_{\text{HOMO}}$ and $A = -E_{\text{LUMO}}$. The ionization potential A and an electron affinity I of our molecule 2MAMP calculated by B3LYP/6-31G(d,p) method is 0.6710eV and 5.6971eV respectively.

TABLE 9. Energy values of 2MAMP by B3LYP/6 31g(d,p) method

Energies	values
E_{HOMO} (eV)	-5.6971
E_{LUMO} (eV)	-0.6710
$E_{\text{HOMO}} - E_{\text{LUMO}}$ gap (eV)	-5.0260
Chemical hardness (η)	2.5130
Softness (S)	0.1925
Chemical potential (μ)	-3.2088
Electronegativity (χ)	3.1840
Electrophilicity index (ω)	2.0171

The calculated values of the Chemical Hardness, Softness, Chemical potential, Electronegativity and Electrophilicity index of our molecule 2MAMP is 2.5130, 0.1925, -3.2088, 4.2692 and 3.1840 respectively as shown TABLE 9. Considering the chemical hardness, large HOMO-LUMO gap represent a hard molecule and small HOMO-LUMO gap represent a soft molecule. From the Table 9, it is clear that the molecule under investigation is very hard since it has a large HOMO-LUMO gap and also having a very small value for softness.

VII. Nonlinear optical (NLO) effects

The NLO activity provide the key functions for frequency shifting, optical modulation, optical switching and optical logic for the developing technologies in areas such as communication, signal processing and optical interconnections [57]. The first static hyperpolarizability (β_0) and its related properties (β , α_0 and $\Delta\alpha$) have been calculated using B3LYP/6-31G(d,p) level based on finite field approach. In the presence of an applied electric field, the energy of a system is a function of the electric field and the first hyperpolarizability is a third rank tensor that can be described by a $3 \times 3 \times 3$ matrix. The 27 components of the 3D matrix can be reduced to 10 components because of the Kleinman symmetry [58]. The matrix can be given in the lower tetrahedral format. It is obvious that the lower part of the $3 \times 3 \times 3$ matrices is a tetrahedral. The components of β are defined as the coefficients in the Taylor series expansion of the energy in the external electric field. When the external electric field is weak and homogeneous, this expansion is given below:

$$E = E_0 - \mu_\alpha F_\alpha - \frac{1}{2} \alpha_{\alpha\beta} F_\alpha F_\beta - \frac{1}{6} \beta_{\alpha\beta\gamma} F_\alpha F_\beta F_\gamma + \dots$$

Where E_0 is the energy of the unperturbed molecules, F_α is the field at the origin, μ_α , $\alpha_{\alpha\beta}$ and $\beta_{\alpha\beta\gamma}$ are the components of dipole moment, polarizability and first hyperpolarizability, respectively.

The total static dipole moment μ , the mean polarizability α_0 , the anisotropy of the polarizability $\Delta\alpha$ and the mean first hyperpolarizability β_0 , using the x, y and z components are defined as:

Dipole moment is

$$\mu = (\mu_x^2 + \mu_y^2 + \mu_z^2)^{1/2}$$

Static polarizability is

$$\alpha_0 = (\alpha_{xx} + \alpha_{yy} + \alpha_{zz})/3$$

Total polarizability is

$$\Delta\alpha = 2^{-1/2} [(\alpha_{xx} - \alpha_{yy})^2 + (\alpha_{yy} - \alpha_{zz})^2 + (\alpha_{zz} - \alpha_{xx})^2 + 6\alpha_{xz}^2]^{1/2}$$

First order hyperpolarizability is

$$\beta = (\beta_x^2 + \beta_y^2 + \beta_z^2)^{1/2}$$

$$\text{Where } \beta_x = (\beta_{xxx} + \beta_{xyy} + \beta_{xzz}), \beta_y = (\beta_{yyy} + \beta_{yzz} + \beta_{yxx}) \text{ And } \beta_z = (\beta_{zzz} + \beta_{zxx} + \beta_{zyy})$$

$$\beta = [(\beta_{xxx} + \beta_{xyy} + \beta_{xzz})^2 + (\beta_{yyy} + \beta_{yzz} + \beta_{yxx})^2 + (\beta_{zzz} + \beta_{zxx} + \beta_{zyy})^2]^{1/2}$$

Since the values of the polarizabilities (α) and hyperpolarizability (β) of the Gaussian 09 output are reported in atomic units (a.u.), the calculated values have been converted into electrostatic units (esu) (For α : 1 a.u. = 0.1482×10^{-24} esu; For β : 1 a.u. = 8.639×10^{-33} esu). The mean polarizability (α_0) and total polarizability ($\Delta\alpha$) of our title molecule are -51.2128 a.u. or 75.8971×10^{-24} esu and 10.0042 a.u. or 14.8236×10^{-24} esu respectively. The total molecular dipole moment and first order hyperpolarizability are 1.8749 Debye and 1.16071×10^{-30} esu, respectively and are depicted in Table 10. Total dipole moment of title molecule is approximately 1.4 times greater than that of urea and first order hyperpolarizability is 3 times greater than that of urea (μ and β of urea are 1.3732 Debye and 0.3728×10^{-30} esu obtained by B3LYP/6-31 G(d,p) method. This result indicates the nonlinearity of the title molecule.

Table 10. The electric dipole moment, polarizability and first order hyperpolarizability 2MAMP

Dipole moment, μ (Debye)		Polarizability α			First order hyperpolarizability β		
Parameter	Value	Parameter	a.u.	esu ($\times 10^{-24}$)	Parameter	a.u.	esu ($\times 10^{-33}$)
μ_x	1.4841	α_{xx}	-46.3486	-68.688	β_{xxx}	10.4582	90.3484
μ_y	0.9307	α_{xy}	0.052	0.0771	β_{xxy}	-0.465	-4.0171
μ_z	0.6682	α_{yy}	-49.6932	-73.6545	β_{xyy}	1.9327	16.6966
μ	1.8749	α_{zz}	-2.2094	-3.2743	β_{yyy}	3.2814	28.3481
		α_{yz}	-57.5967	-85.358	β_{xxx}	-4.2015	-3.6297
		α_{zz}	0.1276	0.1891	β_{xyz}	-0.8634	-7.4589
		α_0	-51.2128	-75.8971	β_{yyz}	-1.5338	-13.2505
		$\Delta\alpha$	10.0042	14.8236	β_{xzz}	-0.8655	-7.4771
					β_{yzz}	-2.2301	-19.2658
					β_{zzz}	-1.2066	-10.4238
					β_{tot}	4.3064	37.2034
					$\beta = (1.16071 \times 10^{-30} \text{ esu})$		

VIII. Conclusion

Based on SQM force field obtained by DFT calculations at B3LYP/6-31 g(d,p) level a complete structural information, FT-IR and FT-Raman vibrational analysis, electronic properties and vibrational properties of 2MAMP have been carried out. The molecular geometry, vibrational frequencies, infrared intensities, Raman activities and Raman intensities of 2MAMP are calculated. The theoretically calculated vibrational modes are compared with experimental values. The experimental values are in good agreement with theoretical values even in the low frequency region. The difference between the observed and scaled wavenumber values of most of the fundamentals is very small. The thermodynamic properties (heat capacity at constant volume, entropy and enthalpy changes) in the temperature ranges from 100 to 1000 K, Rotational constants, a zero point vibrational energy and SCF energy of title compound are calculated and also calculated. The theoretical UV-Visible spectrum was recorded. The ¹H and ¹³C NMR magnetic isotropic chemical shifts were calculated by B3LYP/6-31 g(d,p) basis set. Total dipole moment, Rotational constants, total energy, entropy, heat capacity at constant volume, zero point vibrational energy and SCF energy of title compound are calculated. The difference in HOMO and LUMO energy supports the interaction of charge transfer within the molecule. The MEP map shows that the negative potential sites are around Nitrogen atoms as well as the positive potential sites are around the hydrogen atoms. The greater dipole moment and hyperpolarizability of the title molecule shows the large NLO optical property of the title molecule.

Acknowledgement

The authors are thankful to Sophisticated Analytical Instrumentation Facility (SAIF), IIT, Chennai, for the spectral measurements.

Reference

- [1] Motte Tollet F, Eustatiu G & Roy D, J Chem Phys, 105 (1996) 7448.
- [2] Hajduk, P.H., Bures, M., Praestgaard, J., and Fesik, S.W., J. Med. Chem., 2000, vol. 43, p. 3443.
- [3] Labrie, F., Singh, Sh.M., and Vab Luu-The, USA Patentno. 6933321, 2005..
- [4] X. Chao, X. Zhang, K. Wang, J. Ji and Q. Chen Acta Cryst. (2012). E68, o114.
- [5] Zeitsch K J, The Chemistry and Technology of FurFural and its Many By-Products, Elsevier, 2000.
- [6] M.J. Frisch, G.W. Trucks, H.B. Schlegel, G.E. Scuseria, M.A. Robb, J.R. Cheeseman, G. Scalmani, V. Barone, B. Mennucci, G.A. Petersson, H. Nakatsuji, M. Caricato, X. Li, H.P. Hratchian, A.F. Izmaylov, J. Bloino, G. Zheng, J.L. Sonnenberg, M. Hada, M. Ehara, K. Toyota, R. Fukuda, J. Hasegawa, M. Ishida, T. Nakajima, Y. Honda, O. Kitao, H. Nakai, T. Vreven, J.A. Montgomery Jr., J.E. Peralta, F. Ogliaro, M. Bearpark, J.J. Heyd, E. Brothers, K.N. Kudin, V.N. Staroverov, R. Kobayashi, J. Normand, K. Raghavachari, A. Rendell, J.C. Burant, S.S. Iyengar, J. Tomasi, M. Cossi, N. Rega, J.M. Millam, M. Klene, J.E. Knox, J.B. Cross, V. Bakken, C. Adamo, J. Jaramillo, R. Gomperts, R.E. Stratmann, O. Yazyev, A.J. Austin, R. Cammi, C. Pomelli, J.W. Ochterski, R.L. Martin, K. Morokuma, V.G. Zakrzewski, G.A. Voth, P. Salvador, J.J. Dannenberg, S. Dapprich, A.D. Daniels, O. Farkas, J.B. Foresman, J.V. Ortiz, J. Cioslowski, D.J. Fox, Gaussian Inc., Wallingford, CT, 2009.
- [7] V. Mukherjee, N.P. Singh, R.A. Yadav, J. Mol. Struct. 988 (2011) 24–34.
- [8] G. Rauhut, P. Pulay, J. Phys. Chem. 99 (1995) 3093–3100.
- [9] P. Pulay, G. Fogarasi, G. Pongor, J.E. Boggs, A. Vargha, J. Am. Chem. Soc. 105 (1983) 7037–7047.
- [10] G. Fogarasi, P. Pulay, in: J.R. Durig (Ed.), Vibrational Spectra and Structure, vol. 14, Elsevier, Amsterdam, 1985, pp. 125–219.
- [11] T. Sundius, J. Mol. Struct. 218 (1990) 321–326.
- [12] T. Sundius, Vib. Spectrosc. 29 (2002) 89–95..
- [13] P.S. Kalsi, Spectroscopy of Organic Compounds, Sixth ed., New Age International (p) Limited Publishers, New Delhi, 2005.
- [14] G. Socrates, Infrared and Raman Characteristic group frequencies, Tables and Charts, third ed., Wiley, Chichester, 2001.
- [15] J.B. Ott, J. Boerio-Goates, Chemical Thermodynamics: Advanced Applications, Calculations from Statistical Thermodynamics, Academic Press 2000.
- [16] N. Prabhavathi, A. Nilufer, V. Krishnakumar Spectrochim. Acta Part A Mol. Biomol. Spectrosc. 114(2013) 101–113
- [17] S. Seshadri, Rasheed M.P., R. Sangeetha, Int. J. Sci. Res. Appl. Chem 8(2015) 87–100
- [18] Molvib (V.7.0) calculation of Harmonic Force Fields and vibrational modes of molecules, QCPE program No. 807, 2002.
- [19] P.S. Kalsi, Spectroscopy of Organic Compounds, Sixth ed., New Age International (p) Limited Publishers, New Delhi, 2005
- [20] G. Socrates, Infrared and Raman Characteristic group frequencies, Tables and Charts, third ed., Wiley, Chichester, 2001
- [21] F.R. Dollish, W.G. Fateley, F.F. Bentley, Characteristic Raman Frequencies of Organic Compounds, John Wiley & Sons, New York, 1997.
- [22] G. Fogarasi, X. Zhou, P.W. Taylor, P. Pulay, J. Am. Chem. Soc. 114(1992) 8191–8201.
- [23] D. Lin-vien, N.B. Colthup, W.G. Fateley, J.G. Grasselli, The Handbook of Infrared and Raman Characteristic Frequencies of Organic Molecules, Academic Press, Boston, 1991.
- [24] M. Diem, Introduction to Modern Vibrational Spectroscopy, Wiley, New York, 1993
- [25] C. James, C. Ravikumar, T. Sundius, V. Krishnakumar, R. Kesavamoorthy, Jayakumar, I. Hubert Joe, Vib. Spectrosc. 47 (2008) 10–20
- [26] K. Fukui, Science 218 (1982) 747–754.
- [27] Mehmet Karabacak, Mehmet Cinar, Mustafa Kurt, Spectrochim. Acta Part A Mol. Biomol. Spectrosc. 74 (2009) 1197–1203.
- [28] D.F.V. Lewis, C. Loannides, D.V. Parke, Xenobiotica 24 (1994) 401–408.
- [29] Z. Zhou, R.G. Parr, J. Am. Chem. Soc. 112 (1990) 5720–5724
- [30] R. Ditchfield, Mol. Phys. 27 (1974) 789–807.
- [31] A.D. Becke, Phys. Rev. 38A (1988) 3098–3100.
- [32] V.G. Malkin, O.L. Malkina, M.E. Casida, D.R. Salahub, J. Am. Chem. Soc. 116 (1994) 5898–5908.
- [33] D.B. Chesnut, C.G. Phung, J. Chem. Phys. 91 (1989) 6238–6245.

- [34] T. Kupka, M. Kolaski, G. Pasterna, K. Ruud, *J. Mol. Struct. THEOCHEM* 467 (1999) 63–78.
- [35] T. Kupka, G. Pasterna, P. Lodowski, W. Szeja, *Magn. Reson. Chem.* 37 (1999) 421–426.
- [36] H.O. Kalinowski, S. Berger, S. Braun, *Carbon-13 NMR Spectroscopy*, John Wiley&Sons, Chichester, 1988.
- [37] K. Pihlaja, E. Kleinpeter (Eds.), *Carbon-13 Chemical Shifts in Structural and Stereochemical Analysis*, VCH Publishers, Deerfield Beach, 1994.
- [38] D. Arul Dhas, I. Hubert Joe, S.D.D. Roy, T.H. Freeda, *Spectrochim. Acta* 77 (2010) 36–44.
- [39] K. Jug, Z.B. Maksic, in: Z.B. Maksic (Ed.), *Theoretical Model of Chemical Bonding*, Part 3, Springer, Berlin, 1991, pp. 233–236.
- [40] S. Fliszar, *Charge Distributions and Chemical Effects*, Springer, New York, 1983.
- [41] E. Smith, *J. Am. Chem. Soc.* 113 (1991) 6029–6037.
- [42] J. Gao, *J. Chem. Phys.* 98 (1993) 1975–1981.
- [43] P. Cieplak, *J. Comp. Chem.* 12 (1991) 1232–1236.
- [44] M. Kurt, P. Chinna Babu, N. Sundaraganesan, M. Cinar, M. Karabacak, *Spectrochim. Acta Part A Mol. Biomol. Spectrosc.* 79 (2011) 1162–1170.
- [45] D. Jacquemin, J. Preat, E.A. Perpète, *Chem. Phys. Lett.* 40 (2005) 254–259.
- [46] D. Jacquemin, J. Preat, M. Charlot, V. Wathelet, J.M. Andre, E.A. Perpète, *J. Chem. Phys.* 121 (2004) 1736–1744.
- [47] M. Cossi, V. Barone, *J. Chem. Phys.* 115 (2001) 4708–4717.
- [48] D. Guillaumont, S. Nakamura, *Dyes Pigments* 46 (2000) 85–92.
- [49] J. Fabian, *Dyes Pigments* 84 (2010) 36–53.
- [50] S. Gunasekaran, R.A. Balaji, S. Kumeresan, G. Anand, S. Srinivasan, *Can. J. Anal. Sci. Spectrosc.* 53 (2008) 149–161.
- [51] J.M.Seminario, *Recent Developments and Applications of Modern Density Functional Theory*, vol. 4, Elsevier, Amsterdam, 1996.
- [52] R.H. Petrucci, W.S. Harwood, F.G. Herring, J.D. Madura, *General Chemistry: Principles & Modern Applications*, ninth ed., Pearson Education Inc., New Jersey, 2007.
- [53] D.A. Kleinman, *Phys. Rev.* 126 (1962) 1977–1979.
- [54] Z. Parr, L. Szentpaly, S. Liu, *Am. Chem. Soc.* 121 (1999) 1922–1924.
- [55] P. Chattraj, B. Maiti, U. Sarkar, *J. Phys. Chem. A* 107 (2003) 4973–4975.
- [56] S.Seshadri, Rasheed.M.P.,R.Sangeetha, *IOSR-J. Appl.Chem* 8(2015) 87-100
- [57] C. Andraud, T. Brotin, C. Garcia, F. Pelle, P. Goldner, B. Bigot, A. Collet, *J. Am. Chem. Soc.* 116 (1994) 2094–2101
- [58] D.A. Kleinman, *Phys. Rev.* 126 (1977) 1962–1979.